ACS APPLIED MATERIALS & INTERFACES

www.acsami.org

Research Article

Stretchable and Skin-Conformable Conductors Based on Polyurethane/Laser-Induced Graphene

Alexander Dallinger, Kirill Keller, Harald Fitzek, and Francesco Greco*

Cite This: *ACS Appl. Mater. Interfaces* 2020, 12, 19855−19865

Read Online

ACCESS | Metrics & More | Article Recommendations | Supporting Information

ABSTRACT: The conversion of various polymer substrates into laser-induced graphene (LIG) with a CO_2 laser in ambient condition is recently emerging as a simple method for obtaining patterned porous graphene conductors, with a myriad of applications in sensing, actuation, and energy. In this paper, a method is presented for embedding porous LIG (LIG-P) or LIG fibers (LIG-F) into a thin (about 50 μm) and soft medical grade polyurethane (MPU) providing excellent conformal adhesion on skin, stretchability, and maximum breathability to boost the development of various unperceivable monitoring systems on skin. The effect of varying laser fluence and geometry of the laser scribing on the LIG micro−nanostructure morphology and on the electrical and electromechanical properties of LIG/MPU composites is investigated. A peculiar and distinct behavior is observed for either LIG-P or LIG-F. Excellent stretchability without permanent impairment of conductive properties is revealed up to 100% strain and retained after hundreds of cycles of stretching tests. A distinct piezoresistive behavior, with an average gauge factor of 40, opens the way to various potential strain/pressure sensing applications. A novel method based on laser scribing is then introduced for providing vertical interconnect access (VIA) into LIG/MPU conformable epidermal sensors. Such VIA enables stable connections to an external measurement device, as this represents a typical weakness of many epidermal devices so far. Three examples of minimally invasive LIG/MPU epidermal sensing proof of concepts are presented: as electrodes for electromyographic recording on limb and as piezoresistive sensors for touch and respiration detection on skin. Long-term wearability and functioning up to several days and under repeated stretching tests is demonstrated.

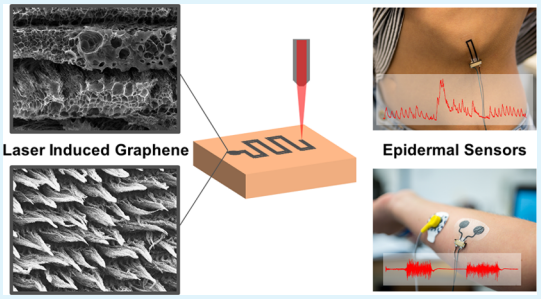

KEYWORDS: *porous graphene, laser, stretchable conductor, epidermal, biosensor*

1. INTRODUCTION

The investigation of materials and processes for obtaining flexible and stretchable conductors has a long history, driven by both scientific curiosity and technological needs. Recently, it has been boosted by the requirements of novel applications in the fields of flexible/stretchable electronics, wearable sensors/devices, epidermal electronics, biointerfaces, soft robotics, prosthetics, actuators, and energy harvesting devices.[1−6] In principle, an "optimal" stretchable conductor would combine the mechanical properties of a typical elastomer material (such as silicone or natural rubber) with the electrical properties of a purely ohmic conductor (as a metal). While the combination of these properties into a single material is very challenging if not impossible, several attempts have been done to realize material systems having at least some of the combined electrical/mechanical features: low tensile modulus, purely elastic behavior up to high values of tensile strain (typ. >20−100% or even more), minimal viscous loss, high toughness, high resilience, low electrical resistivity, minimal or predictable/repeatable change of electrical resistance upon stretching, minimal/no fatigue, and aging under repeated mechanical cycles. A variety of approaches have been investigated so far, including conducting polymers and their composites with cross-linkable elastomers,[7,8] microfabricated serpentine structures of metals,[9] nanofiber/metal flakes composite embedded into a stretchable polymer,[10,11] and surface microwrinkling of metal thin films.[12−14] Their design can be set in order to accommodate a certain preset stretching in the material without failure; however, complex multistep fabrication procedure is often required. Moreover, the introduction of large amounts of stiff or brittle conductive fillers in the soft and stretchable matrix severely changes its mechanical properties. Alternatively, creation of stretchable conductive nanocomposites has been investigated by means of metal nanoparticle implantation into elastomers. Both filtered cathodic vacuum arc metal ion implantation of gold nanoparticles on PDMS[15] and supersonic cluster beam implantation

Received: February 20, 2020
Accepted: April 6, 2020
Published: April 6, 2020

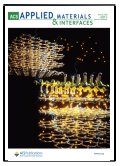

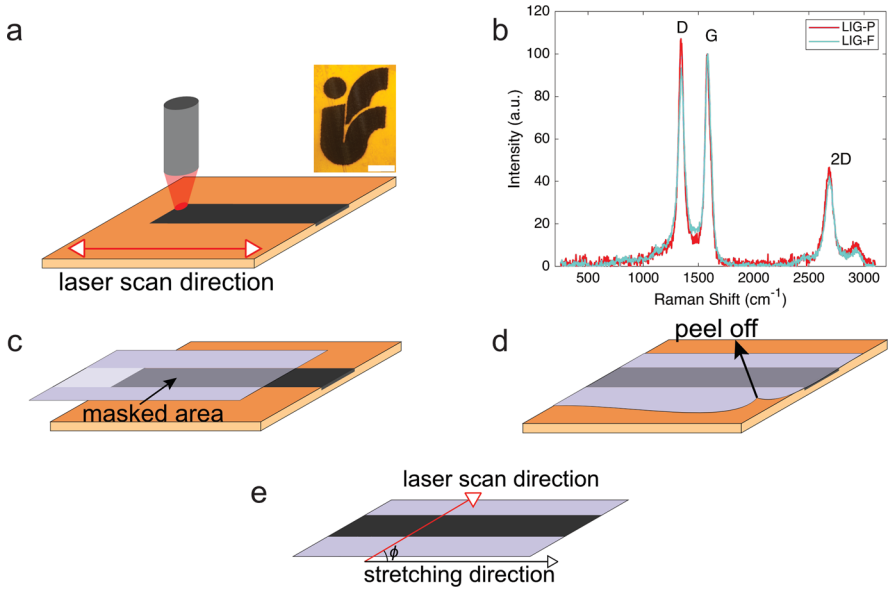

Figure 1. (a) Laser scribing on the PI sheet for LIG creation, inset: LIG scribed into PI representing the logo of our Institute of Solid State Physics, TU Graz (scale bar: 2 mm); (b) Raman spectra of the LIG-P (red) and LIG-F (light blue) samples showing the characteristic D, G, and 2D bands; and (c–e) schematics of LIG transfer on MPU and definition of angle ϕ between laser scan and stretching directions.

of neutral metal nanoparticles onto ionogels[16] have been demonstrated and applied to fabrication of actuators for soft robotics. With the aim to avoid the use of expensive cleanroom techniques or exotic materials and to reduce the overall fabrication complexity, various strategies for printing of metal nanoparticles or other inorganic/organic conductors onto elastomers have been proposed.[17−19] Printing is often followed by heat or flash lamp annealing to attain sintering and thus higher conductivity of printed conductors. Printing of carbon nanomaterials, such as graphene sheets and carbon nanotubes, is one of the most promising strategies. Nevertheless, complex chemical processing is needed, for example, for graphene exfoliation and for attaining stable, highly conductive dispersions. In 2014, a novel method was reported for the conversion of commercial polymers into conductive porous graphene by direct laser scribing in ambient atmosphere with a commercial CO_2 infrared laser, creating the so-called laser-induced graphene (LIG).[20,21] LIG created by means of such a photothermal process is a 3D porous material exhibiting very high surface area, excellent conductivity, and high thermal stability. Differently from other approaches, the graphene preparation and its patterning and embedding into a polymer substrate is performed in just a single and fast step, without the need for subsequent wet chemical steps. By controlling the laser fluence (i.e., optical energy delivered per surface area), it is possible to create materials with different pore size, thickness of porous structure (from few to hundreds of micrometers), and to control the formation of so-called LIG-forest, made up of dense bundles of long fiber-like LIG.[22] The peculiar graphene structure was investigated in depth revealing a few-layered graphene nature, as evidenced by transmission electron microscopy, Raman, and X-ray diffraction analysis.[20,22] LIG formation from other polymers and even from renewable precursors such as wood, clothes, and food (e.g., coconut shell, bread, and potato skin) has been demonstrated.[23] This latter finding can potentially expand the application of LIG into transient or edible electronics and further drastically reduce the cost and environmental footprint of LIG-based devices. It is evident that graphene-based devices are of a great interest in modern science and technology, and therefore easy-to-implement techniques are highly demanded for their production. Recently, a review summarized the progress made in LIG in the last 5 years.[24] Following the first reports several applications of LIG were proposed, including microfluidics, electrocatalysts, strain sensors,[25] and microsupercapacitors. LIG enables the integration of conductive tracks (sheet resistance down to few Ω/□) into flexible polymer sheets, providing a suitable and attractive approach to printed electronics. Moreover, LIG-derived circuits were transferred onto prestretched elastomers allowing to form complex 2D and 3D hierarchical microarchitectures.[26] In present work, laser-induced pyrolysis of polyimide (PI) sheets, a common substrate used for circuit and electronic devices, is used for producing LIG materials. Tuning of LIG material morphology and properties by different laser processing is investigated through scanning electron microscopy (SEM) imaging, and their composition is assessed by means of Raman spectroscopy. In particular, by varying laser system parameters (i.e., speed, power, focusing of the laser rastering, and determining the actual laser fluence H), it is possible to control the morphology of produced LIG from a "flat" porous graphitic structure (LIG-P) to very long self-aligned carbon nanofibers (LIG-F). A simple method is then proposed for creating LIG stretchable and conformable conductors by lamination transfer of LIG materials from the native PI onto a thin, stretchable, transparent medical grade polyurethane (MPU) with optimal on-skin adhesion and breathability (i.e., permeability to moisture produced by skin transpiration). The influence of laser rastering direction on LIG-P and LIG-F growth and on the electromechanical properties of LIG/MPU composites is discussed. Fabricated LIG/MPU composites show stretchability up to 100% as well as long-term durability in electromechanical tensile tests up to 200 cycles. Three proof of concept epidermal sensing applications of LIG/MPU are presented. A conformable skin-contact dry electrode is tested for electromyography (EMG) recording. On the basis of the

https://dx.doi.org/10.1021/acsami.0c03148
ACS Appl. Mater. Interfaces 2020, 12, 19855−19865

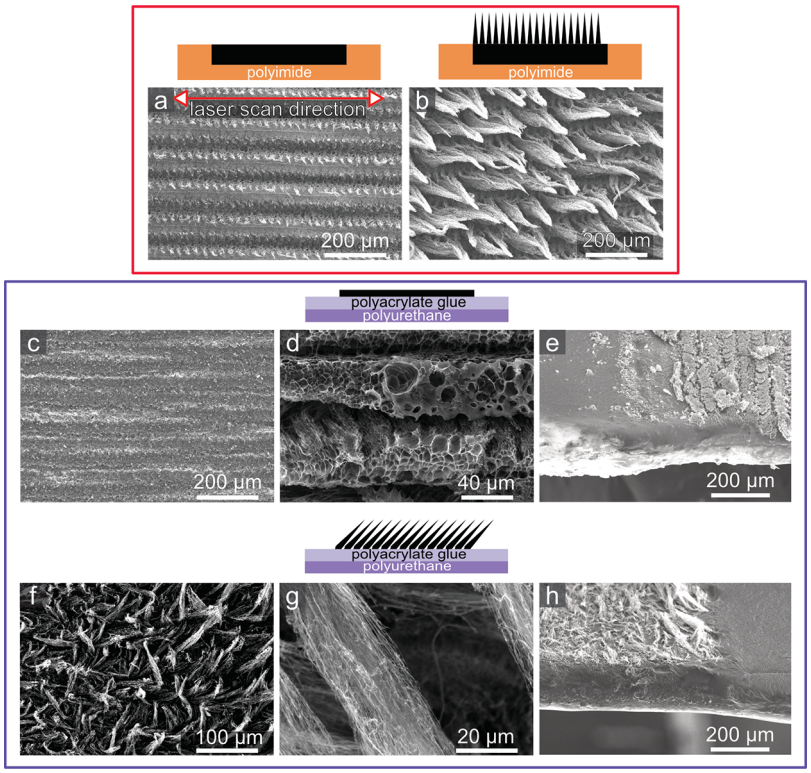

Figure 2. Scheme and SEM images of LIG on PI (top panel) and LIG/MPU (bottom panel): (a) LIG porous (LIG-P) and (b) LIG fibers (LIG-F) on PI; (c,d) morphology and (e) cross-section of LIG-P/MPU; and (f,g) morphology and (h) cross-section of LIG-F/MPU. All SEM images are top view (sample tilt angle $\theta = 0$), except for (e,h) which are tilted views ($\theta = 50°$).

good stability under stretching and of the distinct piezoresistive behavior of LIG/MPU materials, a pressure/touch resistive sensor and a breath monitoring sensor on skin are demonstrated and tested. A method is implemented for obtaining vertical interconnect access (VIA) into sensors, as desired for minimizing typical rupture problems of epidermal devices related to external wiring connectors.

2. RESULTS AND DISCUSSION

With the objective of developing novel epidermal sensors, we investigated LIG synthesis and its integration into a stretchable and conformable carrier, suitable for epidermal applications. Given the requirements of such application, the choice was to use a commercially available medical polyurethane film (MPU) normally used for wound dressing and protection. The MPU is composed of a thin medically approved polyurethane layer coupled with a skin-safe polyacrylate adhesive. An overall MPU thickness of (54 ± 6) μm (polyurethane + polyacrylate glue) was estimated by optical microscopy. The commercially available MPU is laminated between a glassine paper sheet and a release plastic liner for facilitating storage, handling, and release on skin. Schematics of MPU layered structure is provided in Figure S1. MPU has numerous features, making it an optimal substrate for epidermal electronics, which include, among others, reduced thickness, high transparency, stable long-term and conformal adhesion on skin (up to 72 h), large stretchability (over 100%), excellent gas permeability, impermeability to liquid water, off-the-shelf availability in large area format, and ease of manipulation/transfer on skin. Several important figures are summarized in Table S1, Supporting Information. As a matter of fact, the MPU film worn on the skin is barely felt by the user. The mechanical properties of the MPU were studied with a custom tensile testing setup and showed a linear elastic behavior at small strain (5%) and only partial elastic behavior for large (30−100%) strain values (see Supporting Information, Figure S2). Because the relevant strain range in epidermal applications (i.e., related to body movement) is typically lower,[27] the partly non elastic behavior at high strain is not considered a major issue. An elastic modulus of (8.5 ± 0.3) MPa was estimated in the 0−30% strain range. Table S1 summarizes the main features and physical properties of MPU. The process of producing LIG is displayed in Figure 1. The scribing of LIG conductive patterns was performed on top of PI sheets with a laser engraver/cutter equipped with a 30 W CO_2 laser source operating in the rastering mode. PI was chosen because of its known good properties as a precursor for LIG.[28] Moreover, preliminary investigations of a different precursor (polyether ether ketone) showed that LIG produced from this material had inferior electrical and mechanical properties than PI-derived LIG, namely, higher electrical resistance and increased brittleness. The process, very simple and scalable in production, permits the customization of the design and of the processing parameters. In the current work, LIG lines were patterned down to a minimum 100 μm width, by scribing with a laser beam having a nominal diameter of 30 μm. Discrepancy between the beam size and actual size of scribed patterns is ascribed to the fact that the actual area affected by local heating (and pyrolysis) is larger than the irradiated one.[22] By adopting different laser scribing setup (and mainly using a laser beam with smaller diameter), further miniaturization of LIG patterns is in principle possible. However, the lateral resolution of the laser scribing adopted here is deemed suitable for the envisioned applications. It is moreover convenient in terms

https://dx.doi.org/10.1021/acsami.0c03148
ACS Appl. Mater. Interfaces 2020, 12, 19855−19865

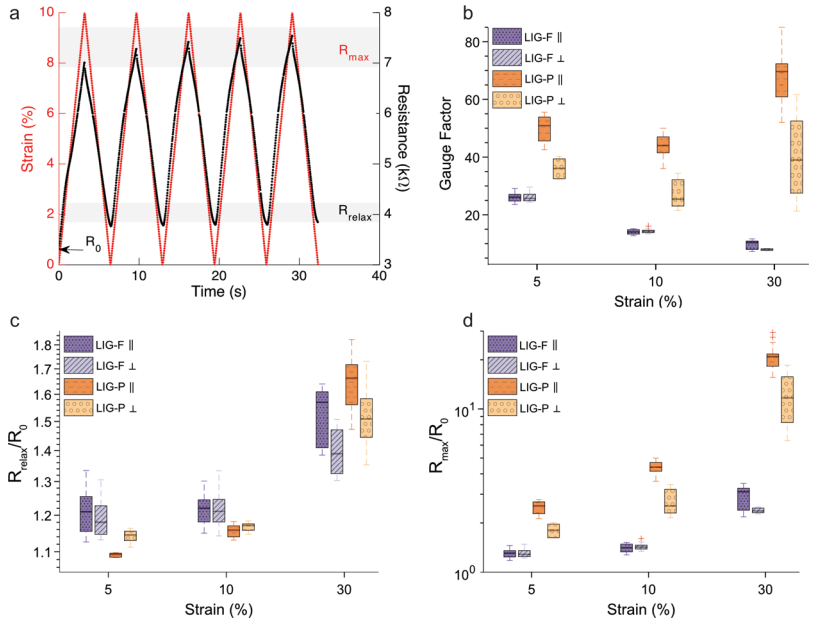

Figure 3. (a) Typical tensile test cycles at 30% strain for LIG-P ⊥/MPU, with definition of R_{max}, R_{relax}, and R_0 and (b) GF, (c) R_{relax}/R_0, and (d) R_{max}/R_0 and their variation vs strain for all tested LIG/MPU composites.

of throughput, an important aspect in view of future scaling up of manufacturing. The composition and surface morphology of LIG materials can be varied by adjusting the laser rastering parameters (resulting in a change of laser fluence H), as detailed in Experimental Section and evidenced in SEM images (Figure 2). Two sets of laser engraver parameters have been selected and used in this study. The first one, corresponding to H = 25 J/cm^2, yields a flat porous graphene structure (LIG-P). Another, corresponding to H = 50 J/cm^2, yields a fiber structure (LIG-F). These optimized H values were set after a preliminary investigation on how the laser scribing parameters influenced LIG formation. To this aim a "map" with different fluence values was created (Figure S3): each point of the map corresponds to a certain set of power and speed of laser rastering; the latter are related to fluence H through eq S1, Supporting Information. In the map, it was possible to distinguish roughly three transitions: one from no or non uniform LIG formation to formation of LIG-P (blue line, $H \approx$ 25 J/cm^2), one from LIG-P to LIG-F (green line, $H \approx$ 45 J/cm^2), and one from LIG-F to destruction of the PI because of too high fluence H (red line, $H \approx$ 80 J/cm^2). Measurements showed that conductivity and thickness of produced LIG increased with increasing H, in agreement with previous findings.[28] On the other hand, the scribed material became increasingly more brittle. Therefore, a tradeoff between conductivity and mechanical stability was made, setting the aforementioned parameters. The composition of the various LIG structures on PI was investigated by means of Raman spectroscopy. The Raman spectra displayed in Figure 1b show a LIG-P (red) and a LIG-F (light blue) sample. Three main features are evidenced: the D band at approximately 1345 cm^{-1} which is associated with disorder and defects in carbon materials, the G band at approximately 1585 cm^{-1}, and the 2D band at approximately 2685 cm^{-1}. The spectrum is clearly evidencing the presence of graphitic carbon for both samples and difference with respect to amorphous carbon.[29] The I_D/I_G intensity ratio is slightly higher for the LIG-P sample, which means that the LIG-F sample has a higher degree of crystallinity (graphitization) than the LIG-P sample.[29] A table with detailed parameters of the Raman bands can be found in the Supporting Information (Table S2). The results for both samples are in agreement with previous findings about similar materials.[22] In addition to providing stable adhesion on skin, the adhesive coating of MPU endowed us with an easy strategy for transfer and embedding of LIG materials, as detailed in the following. In Figure 1c−e, the transfer process with the masked MPU and LIG is shown. The MPU film was laminated onto the scribed LIG patterns, allowing the polyacrylate adhesive stick onto it. By applying different pressures onto the MPU, the LIG paths were then simply transferred onto the MPU carrier when the latter was peeled off. For LIG-P samples, the whole bulk was transferred onto the MPU, while for the LIG-F, only the surface fibers were detached from the PI precursor, leaving behind the bottom-most porous structure. Investigations of the morphology of LIG with an electron microscope show small features for the LIG-P (Figure 2a) and fiber cones consisting of bundles of fibers for LIG-F (Figure 2b). These fibers have an average diameter of around 50−70 nm and a typical length of around 100−200 μm. The morphology of the transferred LIG/MPU is changed (as evidenced in Figure 2c,f) because the bottommost produced LIG is exposed as the topmost. For this reason, the transferred LIG-P surfaces feature a structure with larger pores (detailed view in Figure 2d), whereas in LIG-F, it is shown that during the transfer the fiber cones were not completely destroyed and an interconnected network of fibers/fiber bundles has been produced. Images of cross-sections (Figure 2e,h) taken at the edge of LIG patterns clearly show that the transferred LIG is not completely embedded into the adhesive layer of the MPU. This is important for some applications where a direct contact between skin and LIG is required. The sheet resistance of the transferred LIG-P, which had a thickness of (8.7 ± 1.4) μm before the transfer, is (100 ± 10) Ω, which is 10 times larger than that before the transfer. This indicates that the structure of the porous graphene gets partly destroyed during the transfer process, despite this could

https://dx.doi.org/10.1021/acsami.0c03148
ACS Appl. Mater. Interfaces 2020, 12, 19855−19865

not be seen in the SEM images. The transferred LIG-F has a sheet resistance of (800 ± 100) Ω. Because the non transferred LIG-F also consists of a porous bulk part which is the main conductor, a comparison of the transferred and non transferred LIG-F would not be meaningful. With regard to LIG-F, it is somehow difficult to provide an estimate of thickness because of the complex morphology of the fibers (e.g. their bending, density, partial alignment) and of the rough surface of the sticky MPU side. In the laser rastering used for production of LIG, the precursor surface is irradiated line by line along the x axis, leading to conversion of the PI into LIG through a photothermal process. Thus, it is reasonable to assume that orientation of the pattern will affect the formed LIG morphology and topography and in turn its mechanical and electrical properties as a stretchable conductor. For this reason, we investigated how the orientation of the produced LIG lines with respect to the stretching direction (i.e., angle ϕ between the rastering direction and the stretching direction, Figure 1e, perpendicular ($\perp$) $\phi = 90°$, parallel ($\parallel$) $\phi = 0°$) affected the LIG and LIG/MPU composites. SEM investigations show that the scribing direction affected the morphology of the produced LIG, as shown in Figure 2a. This effect is more present in the LIG-P because of its bulky nature.

The electromechanical behavior of the LIG/MPU composites was investigated in depth with a custom setup, which enabled a simultaneous tensile testing and resistance measurement of stretchable conductors. The same tensile test protocol was performed on all the samples: 5 cycles of stretch/relax for each preset level of maximum strain. Maximum strain was set at ϵ = 5, 10, and 30%, followed by a final single stretch at ϵ = 100% LIG-P/MPU and LIG-F/MPU samples with parallel and perpendicular orientation tested and their behavior compared (Figure 3b–d). An example of a typical experiment (10% strain stretching, repeated 5 times) is reported in Figure 3a for the sample LIG-P $\perp$/MPU. The corresponding trend of force versus strain for repeated cycles did not differ from the one of the bare MPU, as provided in Figure S2. In these measurements, R_0 was defined as the initial resistance of the sample before imposing a stretching at a certain strain level. R_{max} was defined as the resistance value at maximum strain for each strain level imposed. R_{relax} was defined as the resistance value obtained upon relaxation (ϵ = 0%) from a set strain value. An example of these quantities is provided in labels in Figure 3a. The values of initial resistance R_0 measured before tensile testing for the different sample types are reported in Table 1.

Table 1. Initial Resistance R_0 for the Different LIG/MPU Sample Types before First Measurement Averaged over at Least Three Samples (Sample Geometry: 30 × 5 mm² Stripes)

sample type	R_0/kΩ
LIG-P $\perp$/MPU	3.1 ± 0.2
LIG-P $\parallel$/MPU	0.9 ± 0.1
LIG-F $\perp$/MPU	16.2 ± 6.2
LIG-F $\parallel$/MPU	12.6 ± 6.5

The overall higher resistance of LIG-F compared to the LIG-P was caused by the different thickness of the two LIG variants as well as the very different morphologies establishing different percolative paths. The lowest resistance among samples is measured with LIG-P $\parallel$, due to the alignment of the produced LIG-P lines along the stretching (and electrical measurement) direction. The laser process produces lines of LIG-P which are very conductive in the direction of rastering. These lines are separated by a less conductive variant of LIG,[23] resulting in anisotropic conductivity. Indeed, higher resistance was measured along a direction perpendicular to the laser rastering in LIG-P. The laser rastering direction was found to have a less important role in LIG-F/MPU materials: LIG-F $\parallel$ and LIG-F $\perp$ showed a smaller relative difference in R_0 (Table 1) and similar change of resistance upon applied strain (Figure 3d). Indeed, even though the partial alignment of as-produced nanofibers on PI could suggest for a stronger orientation effect (Figure 2d), this alignment is lost during the transfer onto MPU (Figure 2e). The relative resistance R_{max}/R_0 for the stretched state for each set strain value shows that LIG-P/MPU has a larger response to strain than the LIG-F/MPU (Figure 3d) over the whole investigated strain range. Stretching LIG-P/MPU to high strain values (up to ϵ = 100%) results in a sudden breakdown at around ϵ = 60% over which the material is not conductive anymore (Figure S4). Nevertheless, upon strain relaxation, a recovery of functionality is observed, despite a partial irreversible loss of conductivity. On the other hand, a continuous increase in resistance with strain is observed for LIG-F/MPU, with no evidence of rupture or breakdown up to ϵ = 100% (Figure S5). This can be explained by differences in the morphology of the two species. LIG-F is composed of individual nanofibers which interconnect with each other and form a percolative conductive network. When this network is exposed to stress, it is not destroyed but has fewer points of overlapping, as shown in Figure 4a,b. LIG-P is instead a bulk of porous graphene which, when under stress, starts to form cracks. Comparing the two species $\parallel$ (Figure 4c) and $\perp$ (Figure 4d) with each other, it is evident that more cracks are formed in LIG-P $\parallel$ due to the alignment of the pattern along the stretching direction. The second row in Figure 4 displays the MPU composites after 30% strain cycles repeated 200 times. For the LIG-P/MPU composite, it is evident that more cracks were formed but are mostly closed after relaxing. For LIG-F, no evidence for destruction can be found. The differences among LIG-P with different orientations and LIG-F composites are emerging even more clearly when the gauge factor (GF) is considered (Figure 3b), which is defined as

$$\mathrm{GF} = \frac{\Delta R/R_0}{\Delta L/L_0} \tag{1}$$

where $\Delta R = R_{max} - R_0$ is the change in resistance measured for a set strain $\epsilon = \Delta L/L_0$, with $\Delta L = L_{max} - L_0$ being the change in length of a sample having a relaxed length L_0. The difference in the GF for LIG-P $\parallel$ and $\perp$ is very evident and is in good agreement with the observation of the SEM images in Figure 4. LIG-P/MPU showed a GF around two times larger than LIG-F/MPU, which increases with increasing strain. The observed maximum value 70 for the GF makes this material an interesting candidate for developing strain sensors. On the other hand, the GF of LIG-F/MPU decreases with increasing strain, probably due to the effect of a partial alignment of fibers along the stretching direction upon repeated tensile exercise. This effect leads in turn into lower sensitivity to strain (see also long-term behavior description in the following). It is important to notice that typically R_{relax} is larger than R_0 (Figure 3c) as it reflects the instantaneous response of the stretchable conductor. Actually, R_{relax} could become lower and

https://dx.doi.org/10.1021/acsami.0c03148
ACS Appl. Mater. Interfaces 2020, 12, 19855−19865

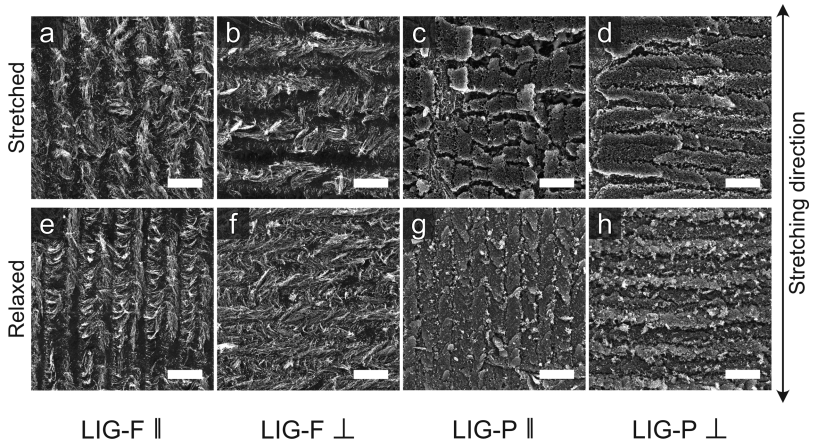

Figure 4. Effect of stress on LIG/MPU. SEM images of samples under stretching: (a) LIG-F ∥, (b) LIG-F ⊥, (c) LIG-P ∥, and (d) LIG-P ⊥. (e–h) Corresponding images of relaxed samples after 200 cycles of 30% strain. Scale bar: 100 μm.

lower and eventually almost recover the initial R_0 value when the sample was allowed to fully relax (i.e., waiting for several tens of seconds at the relaxed position, e.g. Figure S6). This phenomenon can be rationalized by taking into account the aforementioned viscoelastic behavior of the MPU, as evidenced in tensile testing experiments (Figure S2). In order to prove that the viscoelasticity of MPU is responsible for the observed resistance change, a dedicated experiment was carried out. A sample was stretched up to 60% strain and then relaxed to 0% strain, while the resistance (and the force) were monitored on a longer timescale with respect to the aforementioned electromechanical tests, allowing for full stress relaxation. An exponential decrease of resistance R over time to the initial R_0 was observed, while a simultaneous decrease in force was detected due to stress relaxation, a typical feature of viscoelastic materials. An exponential fit permitted to estimate a time constant $\tau = (18.5 \pm 2.8)$ s for both the force and resistance, evidencing the correlation of resistance change with the stress relaxation of the MPU (Figure S7a–c). Thus, R_0 should be rather seen as the equilibrium resistance value, describing a proper fully relaxed state, instead of R_{relax}. The evolution of R_0 with increasing strain levels is shown in Figure S8. A small irreversible variation of R_0 is observed, much smaller than the one assessed in a short time scale measurement by means of the quantity R_{relax}. The relative resistance R/R_0 for the relaxed state in Figure 2c shows that the LIG-F/MPU have a higher variation and value for small strain values. Comparing this with the initial resistance R_0 opens the question why Figure S8 shows nearly no variation of R_0 over strain. An electromechanical testing over 200 cycles at 30% strain was carried out to investigate the long-term behavior of LIG-F/MPU and LIG-P/MPU composites. Figure S9 Supporting Information displays the relative resistance in the stretched (R_{max}/R_0) and relaxed states (R_{relax}/R_0). The results suggest that the LIG-F/MPU samples do not get degraded but rather show an enhancement of conductivity upon exercising, possibly due to alignment of nanofibers along the stretching direction upon repeated tensile testing. However, the LIG-P/MPU samples showed an increase in resistance with increasing strain cycle number at an imposed max strain of 30%. This is related to the crack formation shown in Figure 4. Regarding the mechanical properties of the MPU, no change in behavior compared to the initial testing could be observed (Figure S10).

A notable remark about our findings on LIG/MPU composites is that the presence of LIG (either LIG-P or LIG-F and irrespective of orientation) is not noticeably affecting the mechanical properties of the composites. Namely, modulus extracted by stress/strain curves of LIG/MPU (Figure S11) are identical to MPU (Figure S12) over the whole studied strain range. Thus, differently by other approaches to stretchable conductors,[30−32] the introduction of conductive functionality is not impairing the stretchability and softness of the polymer matrix substrate, with obvious benefits toward the development of soft epidermal devices.

2.1. Interconnectivity through VIAs in LIG/MPU Composites. Once the electromechanical behavior of LIG/MPU composites was characterized, we focused our attention onto developing epidermal sensors out of these stretchable conductors. One of the main challenges related to epidermal sensors for personal monitoring based on thin, conformal, stretchable materials is related to their wiring to devices for signal processing (either worn on skin or standard benchtop equipment). Indeed, wiring connections in thin films are prone to failure (rupture) or to unstable and noisy electrical connections when devices are worn on skin. The latter can be due to relative displacement caused by skin stretching or to movements of the subject, giving rise to so-called movement artifacts in the recorded biosignals.[33] These issues are due to intrinsic limitations of material properties (e.g. mismatch of thickness and stiffness at the interface between thin film and wires) and in processing. A possible strategy to overcome these issues is the establishment of VIA through the thin films used. VIAs can also provide further opportunities for multilayer processing to increase the density of integrated electronics and circuits into a small patch-like device on skin. To this purpose, we developed a strategy for VIAs into LIG/MPU composites to electrically connect different layers and enable accessing through the whole MPU down to the lower lying (i.e. skin-contact) layer. The schematics of layers in the VIAs is displayed in Figure 5a. Small holes (diameter $\approx$ 100 μm, Figure 5b) are laser-cut into areas where a VIA connection should be. These holes are small enough to not interfere with the transfer process or drastically change the robustness and stretchability of the MPU. Further miniaturization of holes for VIAs in future applications could be feasible by adopting smaller laser beam size. Once the LIG is transferred onto the MPU with holes, a connection back layer of MPU is laminated

https://dx.doi.org/10.1021/acsami.0c03148
ACS Appl. Mater. Interfaces 2020, 12, 19855−19865

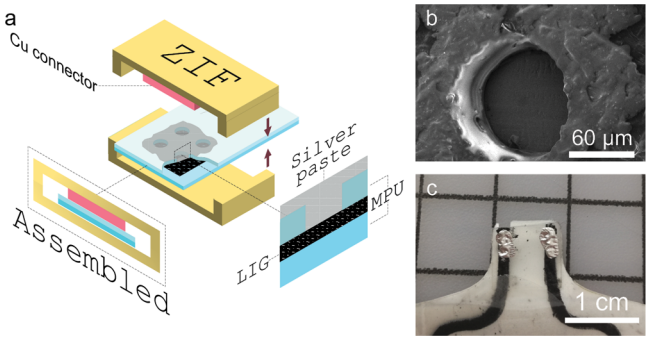

Figure 5. (a) VIA scheme with ZIF-connector for wiring, (b) SEM image of laser-cut holes in the top layer of MPU, and (c) photo of a finished connector with silver ink-filled VIAs.

onto it with an adhesive part facing topward. The purpose of the back layer is to provide encapsulation of LIG and VIA connector and to avoid subsequent sticking on the skin of this part. The holes are then filled with silver ink and dried. Because of the open and porous structure of LIG (having a good wettability), the silver ink spreads into the LIG layer, forming a LIG/Ag composite and ensuring a good connection.[34] With this approach, we were able to create a soft VIA connector design which is only two times thicker than the electrode itself (2 layers of MPU ≈ 100 μm) and has a minor and localized effect in increasing stiffness, and it is robust at the same time. This VIA connector design enabled wiring from the top of the composite (Figure 5c) and not from the bottom, a common configuration in other epidermal devices that introduces several stability issues. This VIA design was used for wiring a zero insertion force (ZIF) connector to all our sensors and always ensured a good electrical connection. The soft VIA connector also sustained a high number of connecting and disconnecting procedures to the ZIF connector without any breakdowns or detachment of the sensor from skin during all our measurements, over several days of use on skin.

2.2. Epidermal Sensors. Three kinds of epidermal sensing with LIG/MPU composites were tested to provide a proof of concept demonstration of applications: (a) an electrophysiology skin-contact dry electrode for surface EMG;[35] (b) a skin-worn piezoresistive sensor for touch/pressure detection; and (c) an epidermal piezoresistive strain sensor for breath monitoring. Other LIG based strain sensors have been proposed recently and showed very interesting performances, such as high GF and long-term stability after repeated deformation. Nevertheless, most of them were relatively thick

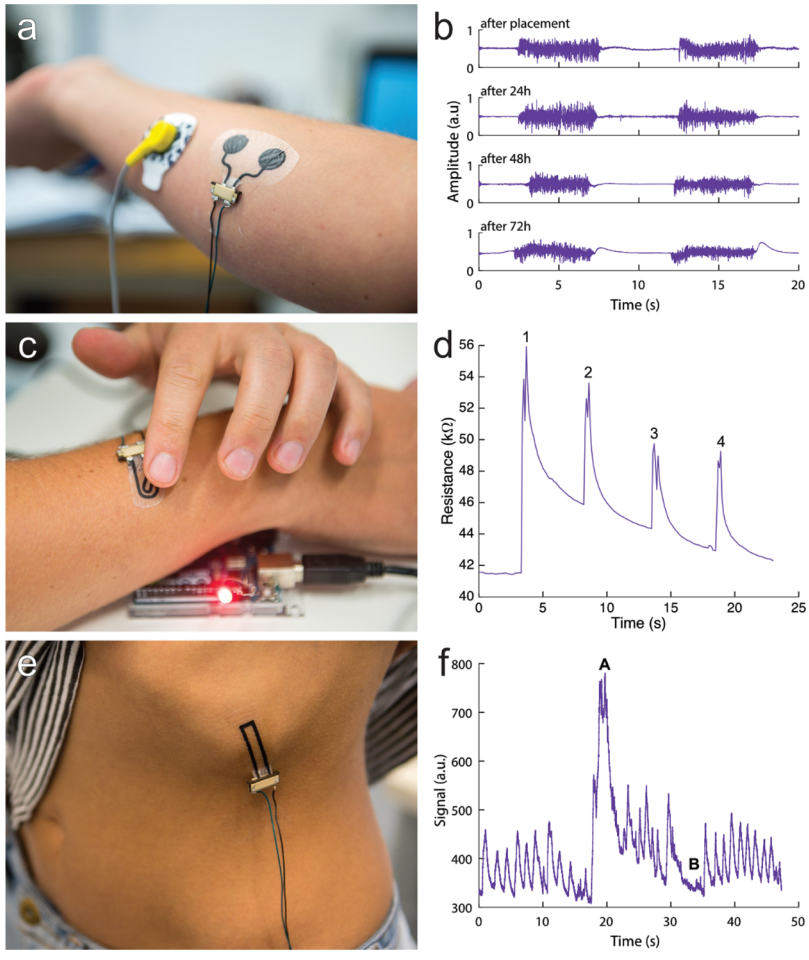

Figure 6. Demonstrations of application of LIG/MPU as epidermal sensors. (a,b) EMG electrodes on forearm and corresponding EMG recordings over 72 h (fist clenching), (c,d) piezoresistive tactile sensor: 1, 2, 3, and 4 pushing onto the button with a finger for switching of a LED, and (e,f) piezoresistive strain/respiration sensor placed on lower left rib cage: A deep inhaling and B holding breath. Video showing the operation of an epidermal tactile sensor is available in Supporting Information.

https://dx.doi.org/10.1021/acsami.0c03148
ACS Appl. Mater. Interfaces 2020, 12, 19855−19865

(several hundreds of μm) and/or stiff; as a consequence, they were not truly conformable to the skin surface and unperceivable for the user, as required for epidermal applications.[36,37] We demonstrated self-adhering electrodes and sensors with an integrated connector terminal with a thickness of under 100 μm which were not only breathable and skin-friendly but also were water-repellent.

2.2.1. EMG Sensor. The LIG/MPU composite could be used as a surface EMG electrode because of its electrical conductivity. This made it possible to detect a change in electrical potential generated by muscle activation at the epidermis surface. An important aspect here was that movement artifacts and change in resistance were kept to a minimum. Based on the electromechanical characterization of LIG/MPU, the material of choice for developing an EMG sensor was LIG-F. The lower GF, the lower thickness, and higher strain tolerance are indeed well-suited for this application. Because the orientation of the fibers (scribing direction) does not have a great impact on the properties of the electrode, it was manufactured with only one rastering direction. The sensor was composed of a couple of circular electrodes, connecting lines, and VIAs for external wiring. It was attached on the forearm of a subject without any skin preparation procedure (e.g., scrubbing and alcohol cleaning) as instead required in other epidermal sensors. It was tested on the skin in combination with a gel-based standard electrode (Ag/AgCl gelled electrode, see details in Experimental Section) used as the reference in EMG recording. The recordings in Figure 6b show the EMG signal recorded from the forearm and related to clenching the fist for 5 s. The electrode placement on the forearm is displayed in Figure 6a. The signal obtained had a good signal-to-noise-ratio (ranging from 10 to 30, see Experimental Section for calculation) and recording stability compared to recording with standard Ag/AgCl electrodes. The electrode was worn for three consecutive days during which the subject had normal daily activities including working in the lab, practicing sports, showering, and sleeping. A small variation in signal quality could be observed over time but only consisted of an increased 50 Hz noise level which was filtered out. After 72 h, an increase in movement noise and decrease in signal reliability could be observed which marked the end of the experiment. During the test period, the electrode was connected and disconnected several times to a monitoring apparatus through the ZIF connector: the soft VIA connector showed no visible signs of degradation or ruptures. The electrode was hardly noticed by the volunteer during the test period because of its thickness, softness, and gas permeability. After removal of the electrode, no skin irritation or allergic reaction was observed.

2.2.2. Tactile Sensing. A second application of LIG/MPU materials can be tactile sensing because of their piezoresistive behavior. The LIG/MPU can be thus used as a sensing device for robotic skins[38] or as an input touch-sensitive device for on-skin electronics, among others. We demonstrated this concept by developing a simple on-skin button which was used to switch a light-emitting diode (LED). An applied pressure onto the piezoresistive LIG/MPU imposed a change in resistance which could be easily detected. The LIG-P was patterned as a connected shape resistor which was used as an on-skin button for demonstration (Figure 6c). The sensor consisted of the LIG-P pattern sandwiched between two MPU layers, so that it was isolated with respect to both the underlying skin and the touching finger. The MPU native adhesive layer provided stable adhesion onto skin. The manufacturing process and connection of the touch sensor was the same as that for the EMG electrode. Optimal wearability was retained, similar to the case of bare MPU. The resistance change was measured and processed by a microcontroller, once a push was detected, an LED was switched. A video of this demonstration can be found in the Supporting Information. The resistance response against tactile inputs (i.e., 4 consecutive contacts by a finger touching the sensor surface) is plotted in Figure 6d and shows very prominent peaks and fast response. The subsequent superimposed exponential decrease was ascribable to the viscoelastic behavior of the MPU, namely, stress relaxation occurring over several seconds (Figures S6 and S7). Although this behavior was not ideal, it could be easily dealt with post processing such as filtering. This could be done because the time scales of the push on the button and the stress relaxation were different. While the latter was actually impairing a fast switching off and recovery of stable R value, as needed for fast and more time resolved touch sensing, the obtained result can enable to envision several applications in electronic skins and wearable devices.

2.2.3. Respiration Sensor. Using the information gained in electromechanical testing of composites, we were able to design a soft and unperceivable epidermal sensor for the detection of the breathing rate (Figure 6e) through strain sensing. For this sensor, LIG-P ‖ was chosen because of its high GF. Similar to the touch sensor, the LIG is sandwiched between two layers of MPU. It was adhered to skin with the native MPU adhesive layer and embedded a VIA soft connector. The sensing principle was based on the expansion in the chest area when breathing; therefore a strain was imposed on a skin-worn conformable sensor.[39] Regular breathing imposed a cyclic tensile strain/relaxation onto the sample resulting in detectable resistance variation in the form of a series of peaks (Figure 6f). By performing simple algorithms like filtering, counting of peaks, and fast Fourier transformation of the electrical signal, it could be possible to extract the information about the respiration rate and filter out movement artefacts (i.e., variation of base resistance level).[40] From the electromechanical testing results (GF of the selected material), we could estimate the strain induced by breathing in the selected body location. The average strain at maximum chest expansion was around 5−7% for which we observed a change of resistance of around $R_{max}/R_0 = 2$, in very good agreement with biomechanical data available in the literature.[41,42]

3. CONCLUSIONS

In this study, we investigated LIG-based stretchable materials produced with an IR laser rastering on top of flexible PI sheets and subsequent LIG transfer onto a medical grade and highly breathable polyurethane (MPU). Either porous (LIG-P) or nanofiber (LIG-F) materials were prepared by changing laser rastering parameters, and their morphology and composition were characterized. A simple strategy for preparing soft, stretchable, skin-mountable LIG/MPU conductive materials is presented. MPU was selected given its excellent properties to act as a skin-contact patch and its excellent mechanical properties. A complete electromechanical characterization of the materials was provided correlating changes in morphology and design of LIG conductors with the observed electromechanical behavior. These stretchable conductors showed quite good conductivity and retained functional properties

https://dx.doi.org/10.1021/acsami.0c03148
ACS Appl. Mater. Interfaces 2020, 12, 19855−19865

upon stretching up to 100%. While the mechanical properties of the soft MPU were not altered by LIG, distinct differences in the electromechanical properties of LIG-P/MPU and LIG-F/MPU were evidenced, permitting to envision future applications in a variety of epidermal sensing scenarios. A simple strategy for providing VIA connectors to LIG/MPU was implemented by means of combined laser cutting and lamination. Three proof of concept demonstrators of skin-mountable sensors based on LIG/MPU were finally discussed. Current findings can open new possibilities toward the development of stretchable nanostructured conductors and epidermal devices through a simple, cheap, and high throughput method, making use of off-the-shelf available materials.

4. EXPERIMENTAL SECTION

4.1. Laser Scribing Parameters. A 10.6 μm CO_2 laser cutter (Universal Laser Systems VLS 2.30, power P_{max} = 30 W) equipped with an HPDFO beam collimator (nominal beam size: 30 μm) was used to create conductive patterns of LIG onto PI (Kapton HN sheets, DuPont, thickness = 50 μm). The laser processing for LIG production was operated in ambient condition, with PI sheets attached onto an Al plate by means of a double-sided adhesive tape. The laser cutter was operated in the raster mode through its native software (Universal Laser System Interface). Two settings of laser rastering parameters were employed for producing LIG-P or LIG-F materials. LIG-P: power = 10%, speed = 10%; LIG-F: power = 20%, speed = 10%. In both cases, settings had a raster resolution of 500 PPI, an image density of 5 (arbitrary scale, defining a spacing between consecutive rastered lines of 280 μm), a positive defocusing of 1 mm. The corresponding laser fluence H was calculated as described in the Supporting Information.

4.2. Characterization. The thickness of the MPU was measured with an Leica Wild M3B optical microscope. The imaging of LIG was performed with a JEOL JSM-6490LV scanning electrode microscope, operating at 5−20 kV acceleration voltage. The electromechanical properties were measured with a custom setup shown in Figure S13. Samples with a dimension of 30 mm × 5 mm were used to measure the resistance response to the imposed strain. Because of the mounting mechanism, the real sample length varied at around 20(2) mm. The electromechanical tensile testing setup was composed of a Load Cell Futek LRF400 and an Amplifier Futek IAA100; the load value was read out with an Arduino microcontroller. The resistance measurement was done with a Keithley 2601B Source Meter sourcing 10 mA. Controlled strain was imposed on samples by means of a NEMA 17 stepper motor controlled by the Arduino microcontroller. A custom C# software was used to send commands to the Arduino and record measurements. The thickness for LIG-P was measured with an AlphaStep D-500 Profilometer from KLA-Tencor. The thickness was estimated to be the same as the missing material in the PI leftover trenches whose depths were measured. Sheet resistance was measured with a custom 4-point probe setup consisting of a Keithley 2602B source meter and four linearly arranged measurement tips with a distance of dprobes = 1.5 mm. Measurements were carried out on square samples with a length of 10 mm. Values reported are averaged over 9 measurements and at least 3 samples. The sheet resistance R_s was calculated with the following equation.

$$R_s = \frac{\pi}{\ln 2} C_f \frac{V}{I} \tag{2}$$

where $\frac{\pi}{\ln 2} C_f = 0.85$ is the correction factor for a finite thin square.

The Raman spectra were measured using a LabRam HR800 combined with an Olympus BX 41 microscope. The laser wavelength was 352 nm (5 mW); an integration time of 4 s × 4 accumulations, a slit/hole size of 200 μm, a 300 lines/mm grating, and an ×50 LMPlanFLN (NA = 0.5) objective were used. The shown spectra are the average of several spectra taken at different positions on the sample, they have been background corrected, and the intensity of the G-band has been normalized.

4.3. Transfer of LIG onto a Stretchable Substrate. The LIG was transferred onto a commercially available MPU (Fixomull transparent, BSN Medical). The MPU, comprising a PU layer and a polyacrylate layer, has two protection liners; the polyacrylate glue side (bottom) is covered with a glassine paper and the top PU side is covered with a plastic support/release liner (See schematics in Figure S1, Supporting Information). For the transfer, the polyacrylate glue on the MPU was masked to match the form of the produced LIG. This was done by cutting the silicon paper with the laser cutter (power = 2.2%, speed = 9%, PPI = 500, ID = 5, defocus of 1 mm) and removing the desired parts. Then, the MPU was put onto the scribed PI, and a pressure (20 g for only fiber transfer and at least 100 g for bulk transfer) was applied with the help of a cotton tip to transfer the LIG.

4.4. Sensor Fabrication. The sensors were made from an electrode body (MPU) and a sensing area (LIG). The LIG was transferred as explained in transfer of LIG onto a stretchable substrate.

4.5. VIAs Fabrication. Once the LIG was transferred, VIAs were fabricated for the external wiring connector. A second layer of MPU was applied to the electrode (leaving out the sensing area in case of the EMG electrode). To establish a connection to the LIG sandwiched between two layers of MPU, small holes with a diameter of around 100 μm were lasered into the upper layer. Holes were then filled with silver conductive paint (Leitsilber 200) to form a connection to the upper layer. The silver paint on top of the holes was also used as a connection point for a ZIF connector. The silver paint was dried for 30 min at 80 °C. When applying the sensor to the skin, the silicon paper liner must be removed and placed onto the skin. Once the sensor is adhered to the skin, the plastic liner can be removed.

4.6. Signal Recording. The EMG signal was recorded with an Olimex ECG shield, consisting of amplifiers and filters and an Arduino microcontroller to record the data. A commercially available pregelled Ag/AgCl electrode (Covidien H124SG, sensing area: 1 cm^2) was placed on the elbow and used as the reference electrode. A single LIG/MPU sensor containing two circle-shaped electrodes (1 cm^2; Figure 6a) was used to record the EMG signal on the forearm while flexing and relaxing the muscles during repeated fist clench maneuver. The resistance measurements for the tactile and respiration sensors were done with a Keithley 2601B Source Meter sourcing 10 mA and a simple voltage divider setup.

4.7. EMG-Signal Processing. The recorded EMG-signal was processed with a 4th order bandstop IIR filter to filter out the 50 Hz noise and its harmonics. Because there is no standard to evaluate EMG signal (S) quality, the calculation of the signal-to-noise ratio (SNR) was in the following way. The EMG feature was separated from the noise by calculating the moving average (MA) over 100 data points and calculating the difference (D) between the (MA) and the signal. The difference was squared, and a threshold value for the feature detection was set. The SNR was calculated by dividing the mean difference of the signal by the mean difference of the noise.

$$D_m = \left[\left(\frac{1}{l}\sum_{i=0}^{l-1} S_{m-i}\right) - S_m\right]^2 \tag{3}$$

$$\mathrm{SNR} = \frac{1}{n}\sum_{m=0}^{n-1} D_{m_{\mathrm{feature}}} \Big/ \frac{1}{n}\sum_{m=0}^{n-1} D_{m_{\mathrm{noise}}} \tag{4}$$

■ ASSOCIATED CONTENT

Supporting Information

The Supporting Information is available free of charge at https://pubs.acs.org/doi/10.1021/acsami.0c03148.

Additional tensile test plots, schematics, SEM images, and tables showing experimental details (PDF)

Operation of an epidermal tactile sensor (MP4)

https://dx.doi.org/10.1021/acsami.0c03148
ACS Appl. Mater. Interfaces 2020, 12, 19855−19865

AUTHOR INFORMATION

Corresponding Author

Francesco Greco − *Institute of Solid State Physics, NAWI Graz, Graz University of Technology, 8010 Graz, Austria;* orcid.org/0000-0003-2899-8389; Email: francesco.greco@tugraz.at

Authors

Alexander Dallinger − *Institute of Solid State Physics, NAWI Graz, Graz University of Technology, 8010 Graz, Austria*

Kirill Keller − *Institute of Solid State Physics, NAWI Graz, Graz University of Technology, 8010 Graz, Austria;* orcid.org/0000-0002-9188-5646

Harald Fitzek − *Graz Centre for Electron Microscopy (ZFE), 8010 Graz, Austria; Institute for Electron Microscopy and Nanoanalysis (FELMI), NAWI Graz, Graz University of Technology, 8010 Graz, Austria*

Complete contact information is available at: https://pubs.acs.org/10.1021/acsami.0c03148

Author Contributions

All authors have given approval to the final version of the manuscript.

Funding

This work was supported by the funding received from the Field of Expertise "Advanced Materials Science" of TU Graz for the Initial Funding project, 11th Call, 2019 by F.G.

Notes

The authors declare no competing financial interest.

ACKNOWLEDGMENTS

The help of Hana Hampel, Alexandra Serebrennikova, Michael Gobald, and Harald Kerschbaumer at the Institute of Solid State Physics of TU Graz is acknowledged.

REFERENCES

(1) Bandodkar, A. J.; Nuñez-Flores, R.; Jia, W.; Wang, J. All-Printed Stretchable Electrochemical Devices. *Adv. Mater.* **2015**, *27*, 3060−3065.

(2) Liu, Y.; Pharr, M.; Salvatore, G. A. Lab-on-Skin: A Review of Flexible and Stretchable Electronics for Wearable Health Monitoring. *ACS Nano* **2017**, *11*, 9614−9635.

(3) Someya, T.; Amagai, M. Toward a New Generation of Smart Skins. *Nat. Biotechnol.* **2019**, *37*, 382−388.

(4) Kaltenbrunner, M.; White, M. S.; Głowacki, E. D.; Sekitani, T.; Someya, T.; Sariciftci, N. S.; Bauer, S. Ultrathin and Lightweight Organic Solar Cells With High Flexibility. *Nat. Commun.* **2012**, *3*, 770.

(5) White, M. S.; Kaltenbrunner, M.; Głowacki, E. D.; Gutnichenko, K.; Kettlgruber, G.; Graz, I.; Aazou, S.; Ulbricht, C.; Egbe, D. A. M.; Miron, M. C.; Major, Z.; Scharber, M. C.; Sekitani, T.; Someya, T.; Bauer, S.; Sariciftci, N. S. Ultrathin, Highly Flexible and Stretchable PLEDs. *Nat. Photonics* **2013**, *7*, 811−816.

(6) Yang, Y.; Deng, Z. D. Stretchable Sensors for Environmental Monitoring. *Appl. Phys. Rev.* **2019**, *6*, 011309.

(7) Wang, Y.; Zhu, C.; Pfattner, R.; Yan, H.; Jin, L.; Chen, S.; Molina-Lopez, F.; Lissel, F.; Liu, J.; Rabiah, N. I.; Chen, Z.; Chung, J. W.; Linder, C.; Toney, M. F.; Murmann, B.; Bao, Z. A Highly Stretchable, Transparent, and Conductive Polymer. *Sci. Adv.* **2017**, *3*, No. e1602076.

(8) Kayser, L. V.; Lipomi, D. J. Stretchable Conductive Polymers and Composites Based on PEDOT and PEDOT:PSS. *Adv. Mater.* **2019**, *31*, 1806133.

(9) Kim, D.-H.; Lu, N.; Ma, R.; Kim, Y.-S.; Kim, R.-H.; Wang, S.; Wu, J.; Won, S. M.; Tao, H.; Islam, A. Epidermal Electronics. *Science* **2011**, *333*, 838−843.

(10) Jin, H.; Nayeem, M. O. G.; Lee, S.; Matsuhisa, N.; Inoue, D.; Yokota, T.; Hashizume, D.; Someya, T. Highly Durable Nanofiber-Reinforced Elastic Conductors for Skin-Tight Electronic Textiles. *ACS Nano* **2019**, *13*, 7905−7912.

(11) Dang, W.; Vinciguerra, V.; Lorenzelli, L.; Dahiya, R. Printable Stretchable Interconnects. *Flexible Printed Electron.* **2017**, *2*, 013003.

(12) Nawrocki, R. A.; Jin, H.; Lee, S.; Yokota, T.; Sekino, M.; Someya, T. Self-Adhesive and Ultra-Conformable, Sub-300 nm Dry Thin-Film Electrodes for Surface Monitoring of Biopotentials. *Adv. Funct. Mater.* **2018**, *28*, 1803279.

(13) Pegan, J. D.; Zhang, J.; Chu, M.; Nguyen, T.; Park, S.-J.; Paul, A.; Kim, J.; Bachman, M.; Khine, M. Skin-Mountable Stretch Sensor for Wearable Health Monitoring. *Nanoscale* **2016**, *8*, 17295−17303.

(14) Palleau, E.; Reece, S.; Desai, S. C.; Smith, M. E.; Dickey, M. D. Self-Healing Stretchable Wires for Reconfigurable Circuit Wiring and 3D Microfluidics. *Adv. Mater.* **2013**, *25*, 1589−1592.

(15) O'Brien, B. M.; Rosset, S.; Anderson, I. A.; Shea, H. R. Ion Implanted Dielectric Elastomer Circuits. *Appl. Phys. A: Mater. Sci. Process.* **2013**, *111*, 943−950.

(16) Santaniello, T.; Migliorini, L.; Yan, Y.; Lenardi, C.; Milani, P. Supersonic Cluster Beam Fabrication of Metal−Ionogel Nanocomposites for Soft Robotics. *J. Nanopart. Res.* **2018**, *20*, 250.

(17) Saidina, D. S.; Eawwiboonthanakit, N.; Mariatti, M.; Fontana, S.; Hérold, C. Recent Development of Graphene-Based Ink and Other Conductive Material-Based Inks for Flexible Electronics. *J. Electron. Mater.* **2019**, *48*, 3428−3450.

(18) Huang, Q.; Zhu, Y. Printing Conductive Nanomaterials for Flexible and Stretchable Electronics: A Review of Materials, Processes, and Applications. *Adv. Mater. Technol.* **2019**, *4*, 1800546.

(19) Li, D.; Lai, W.-Y.; Zhang, Y.-Z.; Huang, W. Printable Transparent Conductive Films for Flexible Electronics. *Adv. Mater.* **2018**, *30*, 1704738.

(20) Lin, J.; Peng, Z.; Liu, Y.; Ruiz-Zepeda, F.; Ye, R.; Samuel, E. L. G.; Yacaman, M. J.; Yakobson, B. I.; Tour, J. M. Laser-Induced Porous Graphene Films from Commercial Polymers. *Nat. Commun.* **2014**, *5*, 5714.

(21) Ye, R.; James, D. K.; Tour, J. M. Laser-Induced Graphene. *Acc. Chem. Res.* **2018**, *51*, 1609−1620.

(22) Duy, L. X.; Peng, Z.; Li, Y.; Zhang, J.; Ji, Y.; Tour, J. M. Laser-Induced Graphene Fibers. *Carbon* **2018**, *126*, 472−479.

(23) Chyan, Y.; Ye, R.; Li, Y.; Singh, S. P.; Arnusch, C. J.; Tour, J. M. Laser-Induced Graphene by Multiple Lasing: Toward Electronics on Cloth, Paper, and Food. *ACS Nano* **2018**, *12*, 2176−2183.

(24) Ye, R.; James, D. K.; Tour, J. M. Laser-Induced Graphene: From Discovery to Translation. *Adv. Mater.* **2019**, *31*, 1803621.

(25) Qiao, Y.; Wang, Y.; Tian, H.; Li, M.; Jian, J.; Wei, Y.; Tian, Y.; Wang, D.-Y.; Pang, Y.; Geng, X.; Wang, X.; Zhao, Y.; Wang, H.; Deng, N.; Jian, M.; Zhang, Y.; Liang, R.; Yang, Y.; Ren, T.-L. Multilayer Graphene Epidermal Electronic Skin. *ACS Nano* **2018**, *12*, 8839−8846.

(26) Ling, Y.; Zhuang, X.; Xu, Z.; Xie, Y.; Zhu, X.; Xu, Y.; Sun, B.; Lin, J.; Zhang, Y.; Yan, Z. Mechanically Assembled, Three-Dimensional Hierarchical Structures of Cellular Graphene with Programmed Geometries and Outstanding Electromechanical Properties. *ACS Nano* **2018**, *12*, 12456−12463.

(27) Maiti, R.; Gerhardt, L.-C.; Lee, Z. S.; Byers, R. A.; Woods, D.; Sanz-Herrera, J. A.; Franklin, S. E.; Lewis, R.; Matcher, S. J.; Carré, M. J. In vivo measurement of skin surface strain and sub-surface layer deformation induced by natural tissue stretching. *J. Mech. Behav. Biomed. Mater.* **2016**, *62*, 556−569.

(28) Lin, J.; Peng, Z.; Liu, Y.; Ruiz-Zepeda, F.; Ye, R.; Samuel, E. L.; Yacaman, M. J.; Yakobson, B. I.; Tour, J. M. Laser-Induced Porous Graphene Films From Commercial Polymers. *Nat. Commun.* **2014**, *5*, 5714.

(29) Ferrari, A. C.; Basko, D. M. Raman Spectroscopy as a Versatile Tool for Studying the Properties of Graphene. *Nat. Nanotechnol.* **2013**, *8*, 235−246.
(30) Gong, S.; Cheng, W. One-Dimensional Nanomaterials for Soft Electronics. *Adv. Electron. Mater.* **2017**, *3*, 1600314.
(31) Kim, D. C.; Shim, H. J.; Lee, W.; Koo, J. H.; Kim, D.-H. Material-Based Approaches for the Fabrication of Stretchable Electronics. *Adv. Mater.* **2019**, 1902743.
(32) Matsuhisa, N.; Chen, X.; Bao, Z.; Someya, T. Materials and Structural Designs of Stretchable Conductors. *Chem. Soc. Rev.* **2019**, *48*, 2946−2966.
(33) *Medical Instrumentation: Application and Design*, 4th ed.; Webster, J. G., Clark, J. W., Eds.; John Wiley & Sons: Hoboken, NJ, 2010; OCLC: ocn259902177.
(34) Rahimi, R.; Ochoa, M.; Ziaie, B. Direct Laser Writing of Porous-Carbon/Silver Nanocomposite for Flexible Electronics. *ACS Appl. Mater. Interfaces* **2016**, *8*, 16907−16913.
(35) Merletti, R. *Electromyography: Physiology, Engineering and Noninvasive Applications*; Wiley-Interscience: Hoboken, N.J., 2010; OCLC: 718181911.
(36) Rahimi, R.; Ochoa, M.; Yu, W.; Ziaie, B. Highly Stretchable and Sensitive Unidirectional Strain Sensor via Laser Carbonization. *ACS Appl. Mater. Interfaces* **2015**, *7*, 4463−4470.
(37) Sun, B.; McCay, R. N.; Goswami, S.; Xu, Y.; Zhang, C.; Ling, Y.; Lin, J.; Yan, Z. Gas-Permeable, Multifunctional On-Skin Electronics Based on Laser-Induced Porous Graphene and Sugar-Templated Elastomer Sponges. *Adv. Mater.* **2018**, *30*, 1804327.
(38) Tee, B. C. K.; Chortos, A.; Berndt, A.; Nguyen, A. K.; Tom, A.; McGuire, A.; Lin, Z. C.; Tien, K.; Bae, W.-G.; Wang, H.; Mei, P.; Chou, H.-H.; Cui, B.; Deisseroth, K.; Ng, T. N.; Bao, Z. A Skin-Inspired Organic Digital Mechanoreceptor. *Science* **2015**, *350*, 313−316.
(39) AL-Khalidi, F. Q.; Burke, R.; Elphick, H.; Tan, S. Respiration Rate Monitoring Methods: A Review. *Pediatr. Pulmonol.* **2011**, *46*, 523−529.
(40) Jeyhani, V.; Vuorinen, T.; Mäntysalo, M.; Vehkaoja, A. Comparison of Simple Algorithms for Estimating Respiration Rate From Electrical Impedance Pneumography Signals in Wearable Devices. *Health Technol.* **2017**, *7*, 21−31.
(41) Wells, J. C. K.; Cole, T. J.; Treleaven, P. Age-variability in Body Shape Associated With Excess Weight: The UK National Sizing Survey. *Obesity* **2008**, *16*, 435−441.
(42) Moll, J. M.; Wright, V. An Objective Clinical Study of Chest Expansion. *Ann. Rheum. Dis.* **1972**, *31*, 1−8.

https://dx.doi.org/10.1021/acsami.0c03148
ACS Appl. Mater. Interfaces 2020, 12, 19855−19865